

# Ferroelectric Localized Field–Enhanced ZnO Nanosheet Ultraviolet Photodetector with High Sensitivity and Low Dark Current

Peng Wang, Yang Wang, Lei Ye, Mingzai Wu,\* Runzhang Xie, Xudong Wang, Xiaoshuang Chen, Zhiyong Fan, Jianlu Wang,\* and Weida Hu\*

Zinc oxide (ZnO) nanosheets have demonstrated outstanding electrical and optical properties, which are well suited for ultraviolet (UV) photodetectors. However, they have a high density of intrinsically unfilled traps, and it is difficult to achieve p-type doping, leading to the poor performance for low light level switching ratio and a high dark current that limit practical applications in UV photodetection. Here, UV photodetectors based on ZnO nanosheets are demonstrated, whose performance is significantly improved by using a ferroelectric localized field. Specifically, the photodetectors have achieved a responsivity of up to  $3.8 \times 10^5 \text{ A W}^{-1}$ , a detectivity of  $4.4 \times 10^{15}$  Jones, and a photocurrent gain up to  $1.24 \times 10^6$ . These device figures of merit are far beyond those of traditional ZnO ultraviolet photodetectors. In addition, the devices' initial dark current can be easily restored after continuous photocurrent measurement by using a positive gate voltage pulse. This study establishes a new approach to produce high-sensitivity and low-dark-current ultraviolet photodetectors and presents a crucial step for further practical applications.

## 1. Introduction

High-performance ultraviolet (UV) photodetectors, with a capability to detect remote UV signals, have been widely used in appli-

Dr. P. Wang, Prof. M. Wu  
School of Physics and Materials Science  
Anhui University  
Hefei 230601, China  
E-mail: mingzaiwu@gmail.com

Dr. P. Wang, Dr. Y. Wang, Dr. R. Xie, Dr. X. Wang, Prof. X. Chen,  
Prof. J. Wang, Prof. W. Hu  
State Key Laboratory of Infrared Physics  
Shanghai Institute of Technical Physics  
Chinese Academy of Sciences  
Shanghai 200083, China  
E-mail: jlwang@mail.sitp.ac.cn; wdhu@mail.sitp.ac.cn

Prof. L. Ye  
School of Optical and Electronic Information  
Huazhong University of Science and Technology  
1037 Luoyu Road, Wuhan, Hubei 430074, China

Prof. Z. Fan  
Department of Electronic and Computer Engineering  
The Hong Kong University of Science and Technology  
Clear Water Bay, Kowloon, Hong Kong, China SAR

DOI: 10.1002/sml.201800492

cations for national defense early warning, navigation, optical information, and other fields.<sup>[1]–[7]</sup> Most of the traditional thin-film UV detectors<sup>[8]–[11]</sup> require a vacuum working environment. They also have other shortcomings, such as a bulky form factor, fragility, high cost, high working voltage, and sensitivity to magnetic fields. These characteristics limit the deployment of UV detection systems in aerospace and high-end warning platforms. With the advancements in materials science, newly developed low-dimensional materials<sup>[12]–[19]</sup> possess ultrathin thickness, and have shown excellent photoelectric conversion characteristics and much improved compatibility with existing microelectronics technology in comparison with the traditional thin-film semiconductors. UV photodetectors based on low-dimensional ZnO have been widely investigated to explore their potential applications due to high specific surface area and

excellent optoelectronic properties, such as high performance at room-temperature, low power consumption, and low cost.

Nanostructure ZnO has a direct wide bandgap (3.4 eV), with many excellent physical and chemical properties, and is one of the most promising candidate materials for UV photodetection. An ultrahigh gain UV photoconductive detector based on a single ZnO nanowire, with a gain of up to  $10^8$ , was demonstrated by Moon et al.<sup>[20]</sup> Jeong et al.<sup>[21]</sup> reported a vertical array of ZnO nanowire UV photodetectors. These detectors can achieve photodetection in the visible and ultraviolet ranges with a photoresponsivity up to  $0.5 \text{ A W}^{-1}$ . Therefore, these impressive results greatly increased the interest of researchers to further study ZnO UV photodetectors. However, these previous studies on low-dimensional ZnO photodetectors mostly exhibited low carrier mobility and high dark current due to their high density of intrinsically unfilled traps and difficult to achieve p-type doping which leads to poor detectivity and, therefore, cannot meet requirements for practical application.<sup>[22]</sup> Fortunately, poly(vinylidene fluoride-trifluoroethylene) (P(VDF-TrFE)) ferroelectric polymer films have been verified to be widely applicable in nanostructure optoelectronic devices to enhance their performance,<sup>[23,24]</sup> providing solutions to address the above issues of nano-ZnO. The function of the ferroelectric film is to introduce a localized electric field to tune the transport properties of the

optoelectronic devices. Therefore, the P(VDF-TrFE) films not only deplete the background charge carriers of ZnO channel, but also act as a surface passivation layer to passivate the naturally unfilled traps of ZnO nanosheets, resulting in high UV-photodetecting performance.

In this work, we demonstrate a high-performance UV photodetector based on ZnO nanosheet with P(VDF-TrFE) as the ferroelectric-driven layer. By introducing a strong ferroelectric localized field, the dark current of the device is suppressed to  $10^{-11}$  A, resulting in the switching ratio of photoresponse increasing to  $10^7$ . A large enhancement in detectivity ( $10^4$  times higher than that of device without depletion) has been achieved due to the ultrastrong ferroelectric localized field. In addition, the initial dark current of the photodetectors can be restored to the original state after their continuous photocurrent has been terminated by applying a positive gate voltage pulse. This increases the repeatability and reliability of the device's photodetection in order to meet requirements for practical applications.

## 2. Results and Discussion

Figure 1a shows the schematic diagram of ZnO nanosheet field-effect transistor (FET) enhanced by a localized ferroelectric field and the thickness of ZnO nanosheet is about 15 nm (more details for ZnO nanosheet characterization can be found in the Supporting Information). In the device, 300 nm thickness P(VDF-TrFE) was selected as the gate dielectric material

and chromium (Cr)/aurum (Au) for the electrodes. In Figure 1b, the output characteristics of the device under dark conditions show good linearity and symmetry, indicating a good Ohmic contact between the Cr/Au electrodes and ZnO. The device was measured at a bias voltage ( $V_{ds}$ ) of 0.1 V in order to study the transfer characteristics, and the result is shown in Figure 1c. A significant positive memory window (about 8 V) is measured when sweeping the gate voltage ( $V_g$ ) from  $-30$  to  $30$  V. The threshold voltages ( $V_{th}$ ) of the device are obtained at the point where  $V_g = -11.2$  V (negative to positive) and  $V_g = -19.1$  V (positive to negative). The  $I$ - $V$  curve reveals a completely counterclockwise hysteresis loop with a high on/off ratio of more than  $10^7$ , which is related to the ferroelectric polarization coercive voltage ( $V_c$ ) of the P(VDF-TrFE) as shown in Figure 1d. The ferroelectric hysteresis loop was measured by an Al/P(VDF-TrFE)/Au capacitor with a voltage swept from  $-60$  to  $60$  V. The maximum remnant polarization field of P(VDF-TrFE) is over  $7 \mu\text{C cm}^{-2}$  with excellent capacitance performance as shown in the inset of Figure 1d.  $V_c$  is located at  $V_g = \pm 20$  V, which is measured with the same thickness of P(VDF-TrFE). Due to the fixed charges and high defect densities at the interface of P(VDF-TrFE)/ZnO, the  $V_{th}$  of the device is smaller and asymmetric in comparison with that of the Al/P(VDF-TrFE)/Au capacitor.<sup>[25]</sup>

In order to investigate the optoelectronic characteristics of ZnO nanosheet photodetector, we conducted a photoresponse measurement with a 375 nm laser under an incident power density of  $8.04 \text{ mW cm}^{-2}$ . Figure 2a displays the

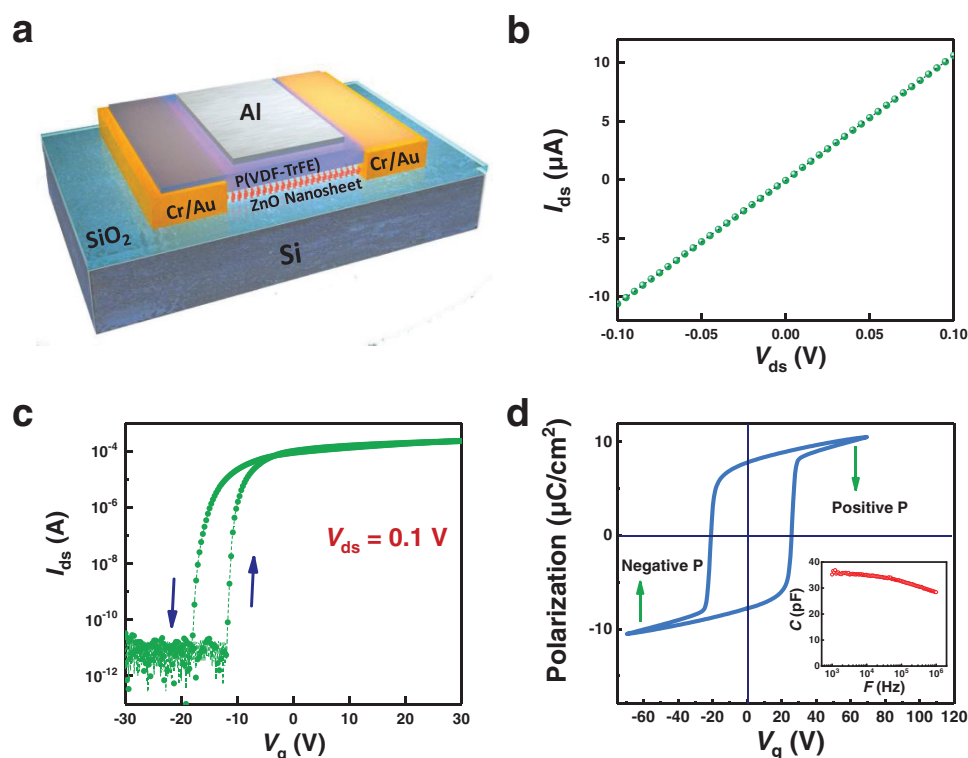


**Figure 1.** Electrical characteristics of ZnO nanosheet field-effect transistor (FET) enhanced by ferroelectric localized field. a) A schematic diagram of ZnO nanosheet FET with P(VDF-TrFE) enhanced by ferroelectric localized field. b)  $I$ - $V$  characteristics of the ZnO FET under dark. c) Transfer characteristics of the ZnO FET at a bias voltage ( $V_{ds}$ ) of 0.1 V. d) Ferroelectric hysteresis loop of an Al/P(VDF-TrFE)/Au capacitor with a voltage sweeping from  $-60$  to  $60$  V, and the corresponding  $C$ - $F$  curve is shown at the inset.

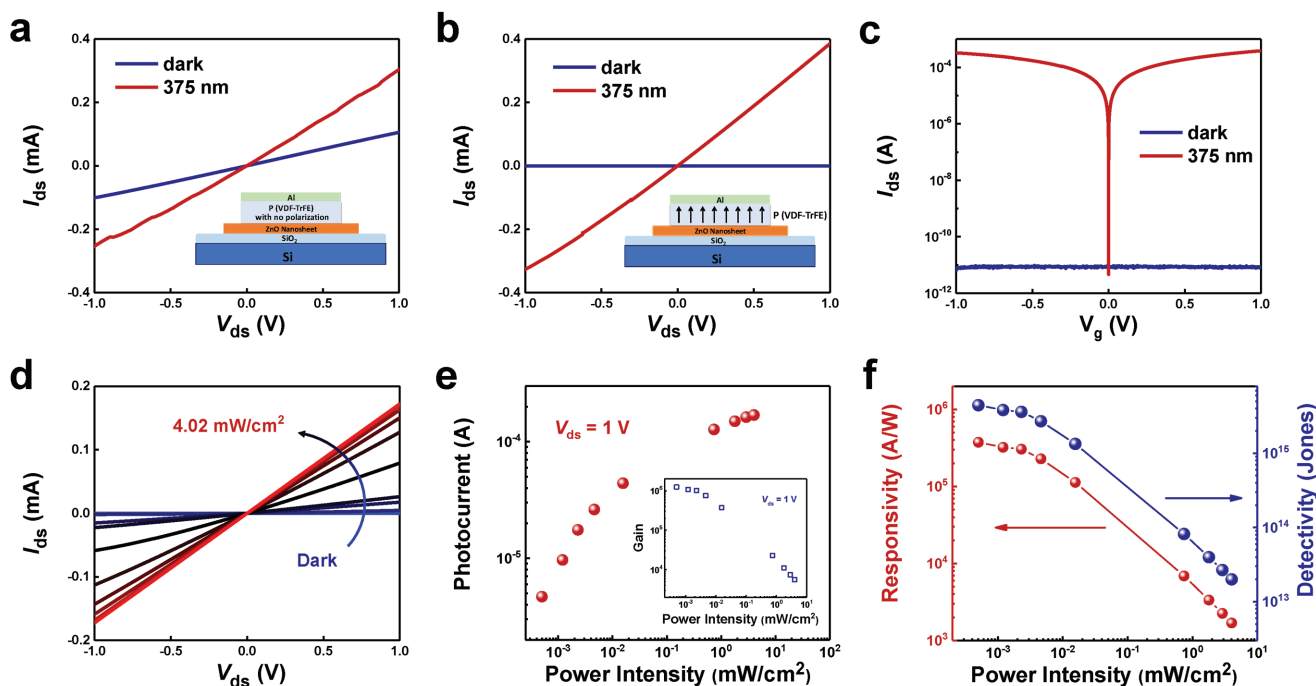


**Figure 2.** Optoelectronic characteristics of ZnO nanosheet photodetector. a) Output characteristics curves of ZnO photodetector under UV illumination with no external electric field applied. b) Output characteristics curves of the device under the negative polarization ferroelectric field, and c) light on/off ratio obtained over  $10^7$  in logarithmic coordinates. d) The output characteristics curves and e) photocurrent of ZnO photodetector under varying incident power density with a wavelength of 375 nm, and the inset shows the calculated  $G$  via varying incident power densities. f) Photoresponsivity and detectivity of the ZnO nanosheet photodetector, showing the maximum  $R$  and  $D^*$  values of  $3.8 \times 10^5$  A W<sup>-1</sup> and  $4.4 \times 10^{15}$  Jones, respectively, when the incident power density is at  $5 \times 10^{-4}$  mW cm<sup>-2</sup>.

output characteristics curves under UV illumination without an external electric field. It indicates that the drain current increases with the increase of bias voltage and the light on/off ratio is only  $\approx 3$ . After the negative polarization ferroelectric field was applied to the device, the output characteristics curves of the device were obtained and are shown in Figure 2b, demonstrating a depletion of the majority carriers in ZnO nanosheets. Due to the fact that the dark current with polarization is  $\approx 10^7$  times smaller than that of without polarization, a  $>10^7$  photocurrent on/off ratio is obtained in logarithmic coordinates as shown in Figure 2c. Because of the strong ferroelectric field induced by the negative polarized P(VDF-TrFE), the dark current of the ZnO nanosheet is greatly suppressed, which has a significant effect on the photoelectric properties of ZnO for use as ultraviolet photodetectors. In addition, we analyzed the results of the photoresponse under varying incident power densities at 375 nm as shown in Figure 2d. Increasing incident laser power density showed that the photocurrent was enhanced monotonically. This is mainly because of increased photon flux illuminating the device, so more electron-hole pairs can be absorbed, and more photocarriers separated under a bias voltage. This results in an increased drain current with increased incident light power.

We also evaluated another figure of merit, specifically photoconductive gain ( $G$ ), which refers to the ratio of the number of carriers collected and the number of absorbed photons in the unit time under illumination. It can be expressed by the following equation

$$G = \frac{N_e}{N_{ph}} = \frac{I_{ph}/e}{PA/h\nu} \quad (1)$$

where  $I_{ph}$  is the photocurrent,  $P$  is the illumination power density,  $A$  is the effective area of the device,  $e$  is the unit charge, and  $h\nu$  is the energy of an incident photon. Figure 2e presents the calculated  $G$  versus incident power densities, and  $G$  is up to  $1.24 \times 10^6$  under an intensity of  $5 \times 10^{-4}$  mW cm<sup>-2</sup>. The high gain indicates that our ZnO nanosheet detector can produce high photocurrent signals under weak illumination conditions. It should be noted that as the UV power density increases, the photoconductive gain decreases gradually due to the saturation of the carrier traps.

The photoresponsivity ( $R$ ) and detectivity ( $D^*$ ) are also important figures of merit for photodetectors, and can be calculated by the following equations

$$R = \frac{I_{ph}}{P} \quad (2)$$

$$D^* = RA^{1/2}/(2eI_{dark})^{1/2} \quad (3)$$

where  $I_{ph}$  is the photocurrent,  $P$  is the illumination power,  $A$  is the effective area of the detector,  $e$  is the unit charge, and the  $I_{dark}$  is the dark current. According to these equations,  $R$  and  $D^*$  values without polarization are  $1.1 \times 10^5$  A W<sup>-1</sup> and  $8.3 \times 10^{11}$  Jones (for more details, please see the Supporting Information), respectively. However, the calculated  $R$  and  $D^*$

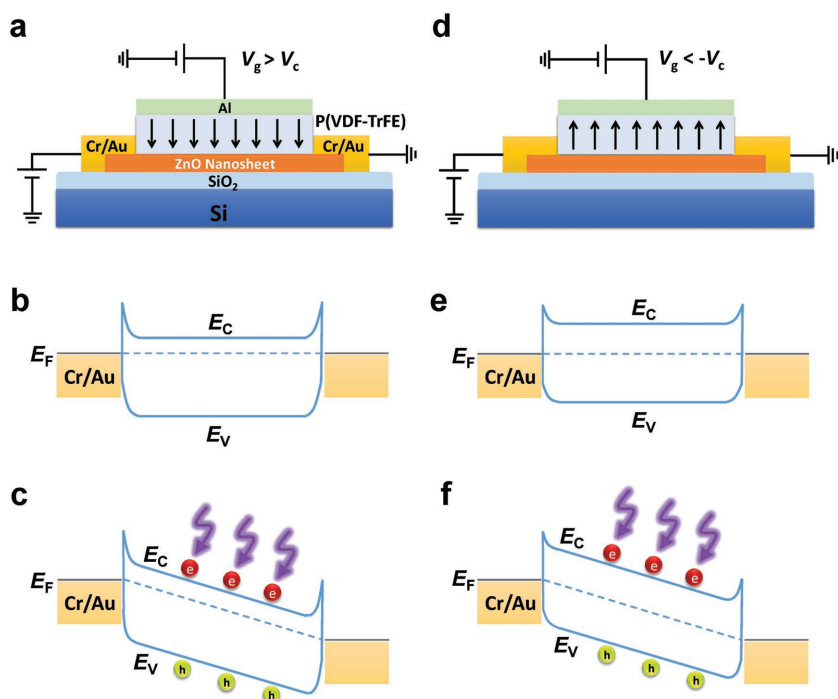


**Figure 3.** Mechanistic diagram of ZnO nanosheet photodetector enhanced by a ferroelectric localized field. a) Structure diagram of ZnO device with negative polarization state. The energy band diagrams of ZnO nanosheet photodetector b) in the dark and c) under illumination. d) Structure diagram of ZnO device with positive polarization state, and the energy band diagrams of the device e) in the dark and f) under illumination.

values are  $3.8 \times 10^5 \text{ A W}^{-1}$  and  $4.4 \times 10^{15}$  Jones under the power intensity of  $5 \times 10^{-4} \text{ mW cm}^{-2}$ , respectively, when the photodetector was depleted as shown in Figure 2f. The  $D^*$  value of the depleted ZnO UV photodetector is more than  $10^4$  times higher than that without depletion, which is mainly due to the fact that the dark current is suppressed to  $10^{-11}$  A.

To better illustrate the effect of P(VDF-TrFE) on the ZnO nanosheet photodetector, a positive voltage is applied to the P(VDF-TrFE) that exceeds its  $V_c$  (Figure 3a), where the domains rapidly turn over and neatly arrange to form a positive remnant polarization electric field in the film. With an increase of the positive polarization electric field of the P(VDF-TrFE), the electron concentration in ZnO nanosheet increases causing elevation of the Fermi level, leading to the increased drain current as shown in Figure 3b. After the UV light illumination, it induces the photogenerated current, which converges the hot electron tunneling current to produce the collected drain current, as shown in Figure 3c. Similarly, the polarization direction is applied by a negative voltage that exceeds  $V_c$ , resulting in a negative polarization electron field as shown in Figure 3d. The strong ferroelectric polarization field generated by the P(VDF-TrFE) can completely deplete the majority carriers in the ZnO channel, leading to its Fermi level being pulled down and the source–drain current under dark substantially being suppressed under the illumination off state (Figure 3e). Under the state of the negative polarization, it results in a full depletion of the intrinsic carriers in the ZnO channel; however, this also produces the larger photogenerated current in the channel compared

with the previously reported nanostructure photodetectors driven by the ferroelectric field (Figure 3f). This is because the ZnO nanosheet has abundant surface state defects, which could capture the photo-carriers to offset part of the photocurrent without an applied external electric field. In addition, the surface state defects of ZnO can be partially passivated by the strong ferroelectric field effect, which makes it possible to form increased photocurrent when illuminated. The ZnO nanosheet device with P(VDF-TrFE) achieves low-level power consumption and dark current in the negative polarization state with the removal of the external applied voltage in contrast to the traditional gate dielectric material. This is the key factor in achieving a high-performance photodetector based on a ZnO nanosheet.

The speed of photoresponse is another important factor to evaluate the performance of photodetectors. To explore the response speed of our device, we measured the performance of the device under the depleted state under ambient conditions as shown in Figure 4a, while maintaining its dark current at a level of  $10^{-11}$  A. As the light illumination turns on, the drain current rises rapidly and reaches saturation at a current level of  $10^{-6}$  A, however the drain current is slightly reduced even if the light is turned off, and it maintains a level that is close to the saturation current for a long time. Because of the abundant oxygen defects in the ZnO crystal, the defect energy levels form in the ZnO bandgap.<sup>[14,26,27]</sup> Moreover, the positively charged oxygen vacancy defects show a strong electron-capture capability and capture the photogenerated electrons. On the other hand, the minority carriers are holes in a n-type ZnO nanosheet; thus, the photogenerated holes can continue to participate in conductivity resulting in a phenomenon of persistent photoconductivity. When the light is turned off, the oxygen chemisorption process dominates and assists photoconductivity relaxation.<sup>[28]</sup> After the light is turned off, the source–drain current is restored to the original level under a backgate voltage pulse of 30 V for 143 ms. Based on the results shown in Figure 4b, the captured rise and fall times of the device are 280 and 440 ms, respectively. This indicates that the reduced electron density of the conduction band leads to a decrease in the photocurrent when the illumination is off. By applying a forward gate voltage pulse, the carrier concentration in the ZnO channel is increased, thus enhancing the probability of the hole recombination in the valence band, which solves the problem of persistent photoconductivity to a certain extent.

In Figure 5, we summarize the performance of ZnO nanosheet photodetectors and our ZnO nanosheet photodetector enhanced by the ferroelectric field. Our device clearly shows advantages compared to previously reported work.<sup>[29–36]</sup>

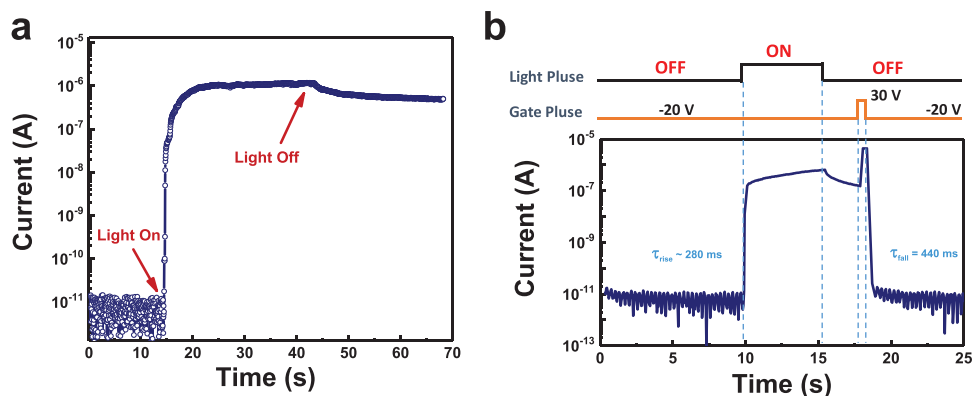


**Figure 4.** Time-resolved photoresponse characterization of ZnO nanosheet photodetector enhanced by a ferroelectric localized field. a) Photoresponse measurement of the ZnO nanosheet under the depleted state. The drain current rises rapidly as the light illumination, and it maintained at the level that is close to the saturation current for a long time even if the light turned off. b) After the light turned off, the current is restored to the original dark current level by providing a positive 30 V backgate voltage pulse to the device for 143 ms. The rise and fall times are reduced to 280 and 440 ms, respectively.

Although most of the UV detectors mentioned above are using an applied external continuous gate voltage to reduce the dark current, leading to the better light switching ratio, these photodetectors are limited by a huge power consumption in practical applications. In addition, there are many reports that confirm the superiority of P(VDF-TrFE) in ferroelectric-FET structure devices. In addition, our devices exhibited superior performance compared to nanostructured ZnO photodetectors composited with other organic ferroelectric films (for more details, please see the Supporting Information). In comparison, our ZnO detector shows excellent optoelectronic performance and ultralow dark current, under ultralow additional power consumption, leading to its far-reaching significance in high-performance wearable photodetector and a wide variety of weapons and equipment.

### 3. Conclusion

Ferroelectric localized field-enhanced FET photodetectors are capable of high-sensitivity and low dark current without external applied gate voltage, resulting in high signal-to-noise ratio (SNR) and low power consumption performance. This is because the extremely strong ferroelectric localized field can effectively deplete the intrinsic carriers of the channel material, leading to the very low dark current to improve SNR of the device. On the other hand, the novel nanostructured (ZnO nanosheet) materials have many excellent properties such as small effective volume, large specific surface area, easiness to modulate the carriers, and high photoelectric conversion capability, which break through the theoretical limits of the photoelectric response of conventional thin-film photodetectors.

In this way, we have fabricated ZnO nanosheet UV photodetectors driven by ferroelectric thin-film P(VDF-TrFE), which integrated the advantages of these two materials and achieved high performance with low power consumption. In this structure, the P(VDF-TrFE) film is used to introduce a localized electric field to deplete the background charge carriers without external applied gate voltage and also acts as a surface passivation layer to passivate the naturally unfilled traps of ZnO nanosheets. In addition, nano-ZnO as the absorption layer in the device has the advantages of natural direct bandgap, large specific surface area, etc., which provide a basic guarantee for high-performance photoresponse. Thus, ZnO nanosheet UV photodetectors driven by P(VDF-TrFE) reveal an improved optical response and detectivity up to  $3.8 \times 10^5 \text{ A W}^{-1}$  and  $4.4 \times 10^{15}$  Jones, respectively. Moreover, the photocurrent gain is  $1.24 \times 10^6$ , which is far better than other ordinary ZnO UV photodetectors. In addition, the photodetector dark current can

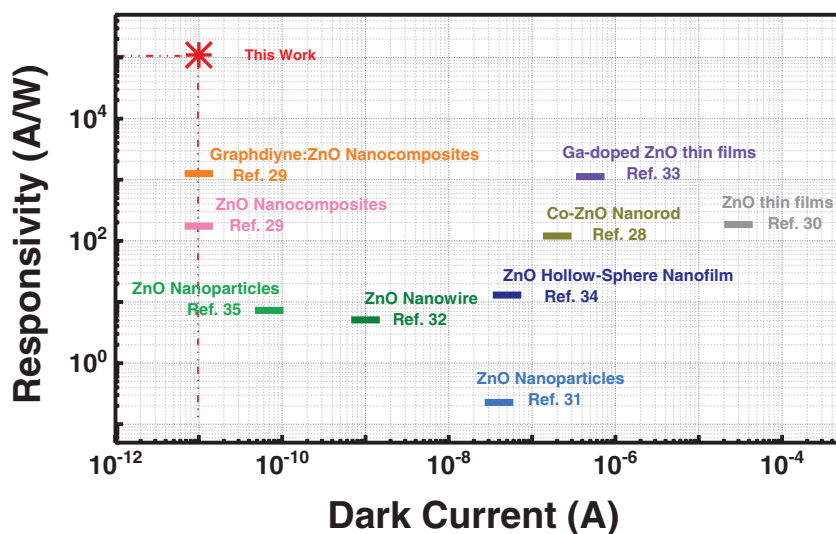


**Figure 5.** Performance comparison of UV detectors based on ZnO. Responsivity (Y-axis) and dark current level (X-axis) of the ferroelectric localized field-enhanced ZnO nanosheet ultra-violet photodetector are comparable and superior to other ZnO detectors.

be restored to the initial state after continuous photocurrent measurement by using a positive gate voltage pulse demonstrating the potential of integrating the ZnO nanosheets with ferroelectrics for novel optoelectronic devices.

#### 4. Experimental Section

**Synthesis and Characterization of ZnO Nanosheet:** The single-crystalline ZnO nanosheets were synthesized via a chemical vapor transport method. Specifically, equal amounts of ZnO (Alfa Aesar 99.99%) and graphite (Alfa Aesar 99.9%) powders with a 2.5% weight percentage of phosphor pentoxide (Alfa Aesar 99.99%) nanopowders were mixed, and carefully ground as the precursors. These powders were loaded into a high-purity alumina boat (Al<sub>2</sub>O<sub>3</sub> 99.5%), while an *a*-plane sapphire substrate coated with 1 nm thick Au film was placed at the surface of the powder source. High purity Ar and O<sub>2</sub>, with flow rates of 70 and 40 sccm, were used as the carrier gases. Then, the powder was heated to 1000 °C with a heating rate of 45 °C min<sup>-1</sup>. After 5 min of growth, the temperature was cooled down to room temperature naturally. All of the ZnO nanosheets were grown under ambient atmospheric pressure.

**Device Fabrication:** To fabricate a ferroelectric localized field-enhanced ZnO ultraviolet photodetector, the as-grown ZnO nanosheets were carefully scraped from the substrate and then ultrasonically dispersed in ethanol. The uniformly dispersed ZnO solution was spin-coated onto a p-type Si/SiO<sub>2</sub> substrate with a SiO<sub>2</sub> layer thickness of 300 nm. Then, the thin layer of methyl methacrylate was spin-coated onto the above-mentioned substrate. Next, the other polymethyl methacrylate layer was fabricated by the same process. Then the electron-beam lithography technique was used to define the source-drain electrodes to fabricate Ti/Au (15 nm/50 nm) electrodes onto the two sides of the ZnO nanosheet. After that, a P(VDF-TrFE) (70:30 mol%) solution was used to fabricate the P(VDF-TrFE) layer on top of the ZnO, with 4 h of heating. Finally, the gate electrode of 10 nm thick aluminum was deposited on top of the P(VDF-TrFE) film.

**Photoelectrical Performance Evaluation:** In photocurrent measurements, a 375 nm laser diode (Thorlabs, LD375P70MLD) was selected as the light source to evaluate the optoelectrical performance. The laser beam was passed through a collimating lens to obtain a parallel beam, and then it illuminated the sample. The photocurrent was produced when the 375 nm laser beam illuminated the ZnO channel, and the signal was recorded by using an Agilent2912 Source Meter instrument. The photoresponse speed was measured by turning the laser on and off using the laser controller (Thorlabs, LDC4001), and the signal was amplified (Stanford, SR570) and detected by a digital oscilloscope.

#### Supporting Information

Supporting Information is available from the Wiley Online Library or from the author.

#### Acknowledgements

P.W. and Y.W. contributed equally to this work. The authors thank James Torley from the University of Colorado at Colorado Springs for critical reading of the paper. This work was partially supported by the National Natural Science Foundation of China (Grant Nos. 11374013, 61704061, and 51672231).

#### Conflict of Interest

The authors declare no conflict of interest.

#### Keywords

dark current, detectivity, ferroelectric localized field, ultraviolet photodetectors, zinc oxide nanosheet

Received: February 5, 2018

Revised: March 19, 2018

Published online: May 2, 2018

- [1] H. Chen, K. Liu, L. Hu, A. A. Al-Ghamdi, X. Fang, *Mater. Today* **2015**, *18*, 493.
- [2] K. Liu, M. Sakurai, M. Aono, *Sensors* **2010**, *10*, 8604.
- [3] L. Sang, M. Liao, M. Sumiya, *Sensors* **2013**, *13*, 10482.
- [4] M. Razeghi, P. Sandvik, P. Kung, D. Walker, K. Mi, X. Zhang, V. Kumar, J. Diaz, F. Shahdipour, *Mater. Sci. Eng., B* **2000**, *74*, 107.
- [5] S. K. Zhang, W. B. Wang, I. Shtau, F. Yun, L. He, H. Morkoç, X. Zhou, M. Tamargo, R. R. Alfano, *Appl. Phys. Lett.* **2002**, *81*, 4862.
- [6] X. Li, C. Gao, H. Duan, B. Lu, Y. Wang, L. Chen, Z. Zhang, X. Pan, E. Xie, *Small* **2013**, *9*, 2005.
- [7] J. H. Jun, H. Seong, K. Cho, B. Moon, S. Kim, *Ceram. Int.* **2009**, *35*, 2797.
- [8] J. Kim, J. Yun, S. Jee, Y. C. Park, M. Ju, S. Han, Y. Kim, J. Kim, W. A. Anderson, J. Lee, J. Yi, *Mater. Lett.* **2011**, *65*, 786.
- [9] S. Liang, H. Sheng, Y. Liu, Z. Huo, Y. Lu, H. Shen, *J. Cryst. Growth* **2001**, *225*, 110.
- [10] M. Liu, H. K. Kim, *Appl. Phys. Lett.* **2004**, *84*, 173.
- [11] Q. A. Xu, J. W. Zhang, K. R. Ju, X. D. Yang, X. Hou, *J. Cryst. Growth* **2006**, *289*, 44.
- [12] L. Ye, P. Wang, W. Luo, F. Gong, L. Liao, T. Liu, L. Tong, J. Zang, J. Xu, W. Hu, *Nano Energy* **2017**, *37*, 53.
- [13] P. Wang, S. Liu, W. Luo, H. Fang, F. Gong, N. Guo, Z. Chen, J. Zou, Y. Huang, X. Zhou, J. Wang, X. Chen, W. Lu, F. Xiu, W. Hu, *Adv. Mater.* **2017**, *29*, 1604439.
- [14] X. Liu, L. Gu, Q. Zhang, J. Wu, Y. Long, Z. Fan, *Nat. Commun.* **2014**, *5*, 4007.
- [15] L. Ye, H. Li, Z. Chen, J. Xu, *ACS Photonics* **2016**, *3*, 692.
- [16] L. Hu, J. Yan, M. Liao, H. Xiang, X. Gong, L. Zhang, X. Fang, *Adv. Mater.* **2012**, *24*, 2305.
- [17] B. Deka Boruah, A. Misra, *ACS Appl. Mater. Interfaces* **2016**, *8*, 18182.
- [18] P. Biswas, S. R. Cho, J. Kim, S. Baek, J. Myoung, *Nanotechnology* **2017**, *28*, 225502.
- [19] H. Li, L. Ye, J. Xu, *ACS Photonics* **2017**, *4*, 823.
- [20] T. Moon, M. Jeong, W. Lee, J. Myoung, *Appl. Surf. Sci.* **2005**, *240*, 280.
- [21] I. S. Jeong, J. H. Kim, S. Im, *Appl. Phys. Lett.* **2003**, *83*, 2946.
- [22] E. M. C. Fortunato, P. M. C. Barquinha, A. C. M. B. Pimentel, A. M. F. Gonçalves, A. J. S. Marques, L. M. N. Pereira, R. F. P. Martins, *Adv. Mater.* **2005**, *17*, 590.
- [23] X. Wang, P. Wang, J. Wang, W. Hu, X. Zhou, N. Guo, H. Huang, S. Sun, H. Shen, T. Lin, M. Tang, L. Liao, A. Jiang, J. Sun, X. Meng, X. Chen, W. Lu, J. Chu, *Adv. Mater.* **2015**, *27*, 6575.
- [24] D. Zheng, J. Wang, W. Hu, L. Liao, H. Fang, N. Guo, P. Wang, F. Gong, X. Wang, Z. Fan, X. Wu, X. Meng, X. Chen, W. Lu, *Nano Lett.* **2016**, *16*, 2548.
- [25] W. Hong, J. I. Sohn, D. Hwang, S. Kwon, G. Jo, S. Song, S. Kim, H. Ko, S. Park, M. E. Welland, T. Lee, *Nano Lett.* **2008**, *8*, 950.
- [26] K. Liu, M. Sakurai, M. Liao, M. Aono, *J. Phys. Chem. C* **2010**, *114*, 19835.
- [27] J. D. Prades, F. Hernandez-Ramirez, R. Jimenez-Diaz, M. Manzanares, T. Andreu, A. Cirera, A. Romano-Rodriguez, J. R. Morante, *Nanotechnology* **2008**, *19*, 465501.

- [28] Z. Fan, P. Chang, J. G. Lu, E. C. Walter, R. M. Penner, C. Lin, H. P. Lee, *Appl. Phys. Lett.* **2004**, *85*, 6128.
- [29] B. Deka Boruah, A. Misra, *ACS Appl. Mater. Interfaces* **2016**, *8*, 4771.
- [30] Z. Jin, Q. Zhou, Y. Chen, P. Mao, H. Li, H. Liu, J. Wang, Y. Li, *Adv. Mater.* **2016**, *28*, 3697.
- [31] S. K. Shaikh, V. V. Ganbavle, S. I. Inamdar, K. Y. Rajpure, *RSC Adv.* **2016**, *6*, 25641.
- [32] E. Amini, M. Dolatyari, A. Rostami, H. Shekari, H. Baghban, H. Rasooli, S. Miri, *IEEE Photonics Technol. Lett.* **2012**, *24*, 1995.
- [33] S. V. Mohite, K. Y. Rajpure, *Opt. Mater.* **2014**, *36*, 833.
- [34] S. S. Shinde, K. Y. Rajpure, *Appl. Surf. Sci.* **2011**, *257*, 9595.
- [35] M. Chen, L. Hu, J. Xu, M. Liao, L. Wu, X. Fang, *Small* **2011**, *7*, 2449.
- [36] N. Nasiri, R. Bo, L. Fu, A. Tricoli, *Nanoscale* **2017**, *9*, 2059.